

Isolated nearly flat higher Chern band in monolayer transition metal trihalides

Kejie Bao,^{1,2} Huan Wang,^{1,2} Jiaxuan Guo,¹ Yadong Jiang,^{1,2} Haosheng Xu,^{1,2} and Jing Wang^{1,2,3,4,*}

¹State Key Laboratory of Surface Physics and Department of Physics, Fudan University, Shanghai 200433, China

²Shanghai Research Center for Quantum Sciences, Shanghai 201315, China

³Institute for Nanoelectronic Devices and Quantum Computing, Fudan University, Shanghai 200433, China

⁴Hefei National Laboratory, Hefei 230088, China

(Dated: May 24, 2024)

The interplay between non-trivial topology and strong electron interaction can generate a variety of exotic quantum matter. Here we theoretically propose that monolayer transition metal trihalides MoF₃ and WX₃ (X= Cl, Br, I) have isolated nearly flat band near the Fermi level with higher Chern number $\mathcal{C} = +3$ and $\mathcal{C} = -2$, respectively. The nontrivial topology of these flat Chern bands originates from the effective sd^2 hybridization of transition metal atom, which transform the apparent atomic d orbitals on a hexagonal lattice into (s, p_+, p_-) orbitals on a triangular lattice. Interestingly, the quantum geometry of flat Chern bands in these materials are comparable with those in moiré systems exhibiting fractional Chern insulator state. The Hofstadter butterfly of such flat Chern bands are further studied. These natural materials, if realized experimentally, could offer new platforms to explore correlated phenomena driven by flat Chern band with higher Chern number.

Introduction— Flat topological band systems have recently received significant attention as platforms to realize exotic correlated states. An outstanding example is fractional Chern insulator state, also called fractional quantum anomalous Hall state, which was experimentally discovered in moiré materials recently in the absence of magnetic field [1–5]. The prerequisites for fractional Chern insulator state is the presence of nearly flat and isolated Chern band with almost ideal quantum geometry [6–18]. Flat topological bands support a lower bound on the superfluid density which otherwise would be zero in flat trivial bands [19], and it was argued to participate in the superconductivity of moiré graphene [20–23]. The experimental demonstration of flat Chern band (FCB) properties has been limited to only a few 2D moiré systems. As such, it is important and interesting to find stoichiometric 2D materials preferably in monolayer with isolated FCB near Fermi level, which could offer new and handier platforms to explore novel quantum states.

Searching for 2D materials that host isolated FCB is challenging because of the complex magnetic structures. It has been understood theoretically that FCB exists in line-graph of bipartite crystalline lattices with spin-orbit coupling (SOC) [24–33]. However, the predicted 2D materials with FCB are quite limited [33–44], and most of them share kagome geometry [45] with Chern number of FCB to be $\mathcal{C} = 1$, mimicking the lowest Landau level. The study of interaction effects in 2D kagome materials faces challenges, the principal of which being electron filling and stability of materials which favor the energetic position of flat band near Fermi level. Meanwhile, to explore new physics beyond lowest Landau level, it is interesting to have a FCB with higher Chern number [46–56]. There remains unclear whether FCB with higher Chern number can exist in realistic natural 2D materials, since generically long-range hopping are need to obtain higher

Chern band with large flatness ratio.

Here we predict monolayer MoF₃ and WX₃ (X= Cl, Br, I) have isolated flat band with higher Chern number near the Fermi level, based on density functional theory (DFT) calculations and tight-binding model. The Vienna *ab initio* simulation package [63] is employed within the strongly constrained and appropriately normed (SCAN) functional [64]. We perform DFT + Hubbard U calculations. The predicted band structure and topology were further verified by Heyd-Scuseria-Ernzerhof (HSE) hybrid functional [65]. MoF₃ and WI₃ are two representative examples, MoF₃ has the ferromagnetic (FM) ground state with Curie temperature to be 28 K, where the valence band is FCB with Chern number $\mathcal{C} = +3$ and bandwidth of about 50 meV. While FCB in WI₃ carries Chern

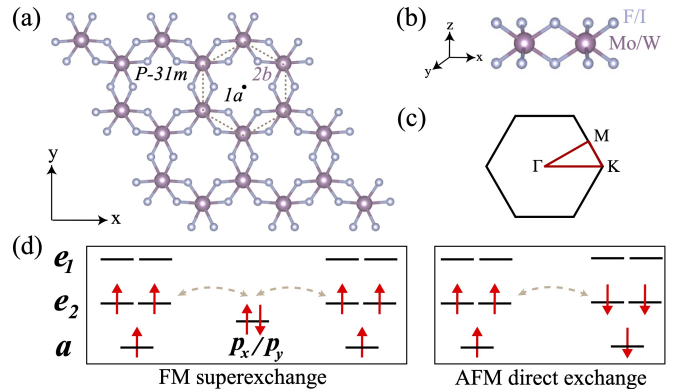


FIG. 1. (a),(b) Atomic structure of monolayer MoF₃/WI₃ from top and side views. The Wyckoff positions $1a$ and $2b$ are displayed (notation adopted from Bilbao Crystallographic Server [57–62]). The key symmetry operations of $P-31m$ include C_{3z} , C_{2y} and inversion symmetry \mathcal{I} . (c) Brillouin zone. (d) Crystal field splitting and schematic diagram of the direct exchange and superexchange between Mo/W d electrons.

	a (Å)	E_B (meV)	\mathcal{C}	$\delta\mathcal{B}$	T	$T_{c/n}$ (K)
MoF ₃	5.65	50	+3	10.04	2.98	$T_c = 28$
WI ₃	7.12	179	-2	1.73	0.1	$T_n = 2.7$
MoCl ₃	6.31	75	-2	0.99	0.74	$T_n < 1$
WCl ₃	6.30	96	-2	1.85	1.25	$T_n = 68$
WBr ₃	6.61	76	-2	1.74	0.31	$T_n = 26$

TABLE I. Lattice constant, bandwidth (E_B), Chern number \mathcal{C} , fluctuation of Berry curvature $\delta\mathcal{B}$, and average trace condition violation T for the topmost valence band; Curie/Néel temperature $T_{c/n}$ from Monte Carlo simulations.

number $\mathcal{C} = -2$ with bandwidth of about 179 meV. Interestingly, the topology originates from the band inversion within strongly hybridized cation d orbitals and anion p orbitals on an effective triangular lattice. The quantum geometry of such FCB are further studied.

Structure and magnetic properties— The monolayer transition metal trihalides have the same honeycomb lattice with the space group $P\bar{3}1m$ (No. 162). As shown in Fig. 1(a), take MoF₃ as an example, each primitive cell includes three atomic layers, where each Mo atoms is surrounded by six F atoms forming a distorted edge-sharing octahedra. Their lattice constants are listed in Table I. We will mainly discuss MoF₃ and WI₃ with similar results for other materials in this class [66]. The dynamical stability of monolayer MoF₃ and WI₃ are confirmed by first-principles phonon calculations [66]. It is worth mentioning that the bulk phase of MoF₃ has been experimentally synthesized [67, 68], which implies high probability to fabricate the 2D phase.

First-principles calculations show MoF₃ has strong FM ground state, while WI₃ has weak zigzag antiferromagnetic (AFM) ground state that is different from previous investigation [69–71]. Both of them have an out-of-plane magnetic easy axis. The underlying mechanism of magnetism can be elucidated from orbital occupation. The distorted octahedral crystal field splits Mo 4d (W 5d) orbitals into three levels, $a(d_{z^2})$, $e_2(d_{x^2-y^2}, d_{xy})$, and $e_1(d_{xz}, d_{yz})$ [Fig. 1(d)]. The energy of a and e_2 stays lower with respect to e_1 , because the latter point towards the negatively charged ligands. Thus each Mo (W) atom is in the $a^1e_2^2$ configuration with the magnetic moment of $3\mu_B$ according to Hund’s rule, which is consistent with the DFT calculations. For nearest neighboring Mo (W) atoms, the FM superexchange from near 90° Mo-F-Mo (W-I-W) bond [72] dominates over AFM direct exchange due to closed e_2^2 subshell. For next-nearest neighboring interaction, FM superexchange dominates for MoF₃, while AFM exchange dominates in WI₃ [66]. Furthermore, the predicted Curie temperature of monolayer MoF₃ is comparable to that of CrI₃ [73]. The Néel temperature for WI₃ is quite low, thus an external mag-

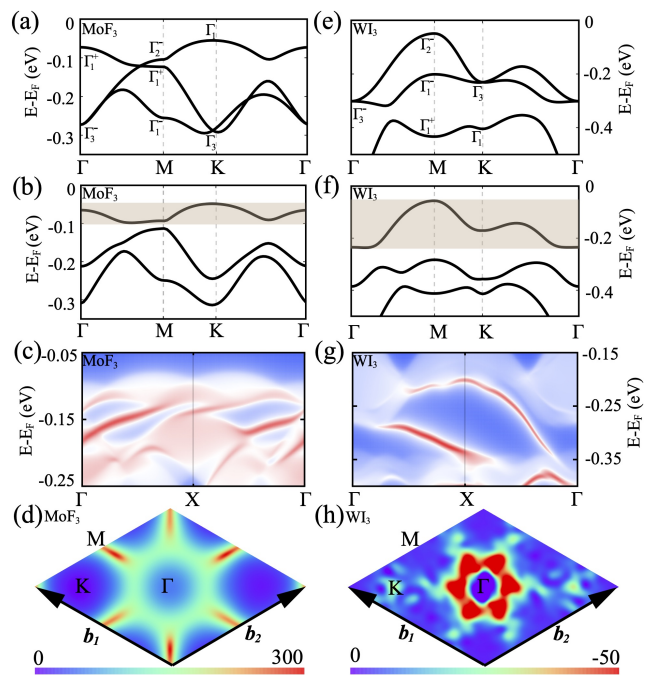


FIG. 2. Electronic structure and topological properties of monolayer MoF₃ and WI₃. (a)-(d) MoF₃, (e)-(h) FM WI₃. The band structure without and with SOC, where the irreducible representation at high symmetry points are shown; topological edge states calculated along the x axis; Berry curvature of the first valence band. The shaded regions in (a) and (e) denote the nearly FCB. The Berry curvature remains the same sign throughout the whole Brillouin zone in both MoF₃ and WI₃.

netic field will drive it into FM state along z axis, where the critical field is about 0.6 T by Monte Carlo simulations [66].

Electronic structures— Fig. 2(a) and 2(b) display the electronic structure of monolayer MoF₃ without and with SOC, respectively. There exists three spin-up bands near the Fermi level which are mainly contributed by Mo d orbitals from a and e_2 levels, and partially from F p orbitals. We calculate the band representation of these three bands and find that they are described by an effective (s, p_+, p_-) basis at Wyckoff positions $1a$ forming a triangular lattice (Table II). There are s - p band inversions around three M points, which is further gapped by SOC. This indicates the nontrivial topology of the first valence band. We further calculate Berry curvature of the valence band and find its Chern number $\mathcal{C} = +3$, which is consistent with three chiral edge states dispersing within the gap below as in the edge local density of states [Fig. 2(c)]. Remarkably, this higher Chern band being consist of localized d orbitals is nearly flat with bandwidth $W \approx 50$ meV, and is also isolated from other bands.

Then we turn to WI₃. Fig. 2(e) and 2(f) display the electronic structure of monolayer FM WI₃ without and

	Γ	M	K
s	$\Gamma_1^+(1)$	$\Gamma_1^+(1)$	$\Gamma_1(1)$
(p_+, p_-)	$\Gamma_3^-(2)$	$\Gamma_1^-(1) \oplus \Gamma_2^-(1)$	$\Gamma_3(2)$

TABLE II. The elementary band representations of space group $P-31m$ for (s, p_+, p_-) orbitals at Wyckoff positions $1a$.

with SOC, respectively. Similar to MoF_3 , three spin-up bands being consist of W d orbitals are near the Fermi level, which are described by an effective (p_+, p_-, s) basis in a triangular lattice from the band representation analysis. Quite different from MoF_3 , the valence bands are p_{\pm} like, and there are double degeneracy at Γ and K points within p_+ and p_- basis, which are further gapped by SOC. Usually, the gap opening from atomic SOC for (p_+, p_-) orbitals on triangular lattices leads to trivial topology [62]. Interestingly, we find Chern number of the first valence band is $\mathcal{C} = -2$ from both the edge state calculations in Fig. 2(g) and Berry curvature in Fig. 2(h). The bandwidth of the Chern band is about $W \approx 179$ meV.

Tight-binding model and analysis of topology— To understand the physical origin of such peculiar electronic structures, we first provide the detailed orbital analysis to demonstrate how the apparent atomic d orbitals on hexagonal lattice transform into (s, p_+, p_-) type orbitals on triangular lattice. The d -orbital projected band structure [66] shows that the natural orbitals d_{z^2} (s -shape when viewed planarly) and $(d_{xy}, d_{x^2-y^2})$ with in-plane characteristics hybridize to form the bands of interest near Fermi level. It is similar to sd^2 hybridization which forms the bonding σ and antibonding σ^* states with trigonal planar geometry [see Fig. 3(a) and 3(b)], having the main contribution towards Wyckoff position $1a$. Interestingly, such hybrid states effectively transform hexagonal symmetry of the atomic Mo/W lattice into the physics of the triangular lattice. The elementary band representation analysis shows that $(d_{z^2}, d_{xy}, d_{x^2-y^2})$ at Wyckoff position $2b$ equals to $(s, p_+, p_-)^{\pm}$ at $1a$ forming triangular lattice, where the other three d bands with (s, p_+, p_-) characteristics are located below the bands of interest [66].

We then construct a concrete tight-binding model to recover the essential topological physics, which applies to both MoF_3 and WI_3 with different parameters. The model consists of $(s^{\uparrow}, p_+^{\uparrow}, p_-^{\uparrow})$ type orbitals at Wyckoff position $1a$ from the band representation in Fig. 2, namely a three-orbital model. The Hamiltonian is obtained by considering the nearest-neighbor and next-nearest-neighbor hopping (namely from Slater-Koster method) with SOC included. As shown in Figs. 3, the band structure and corresponding irreducible representations of high symmetry points in DFT calculation are rebuilt in our tight-binding model.

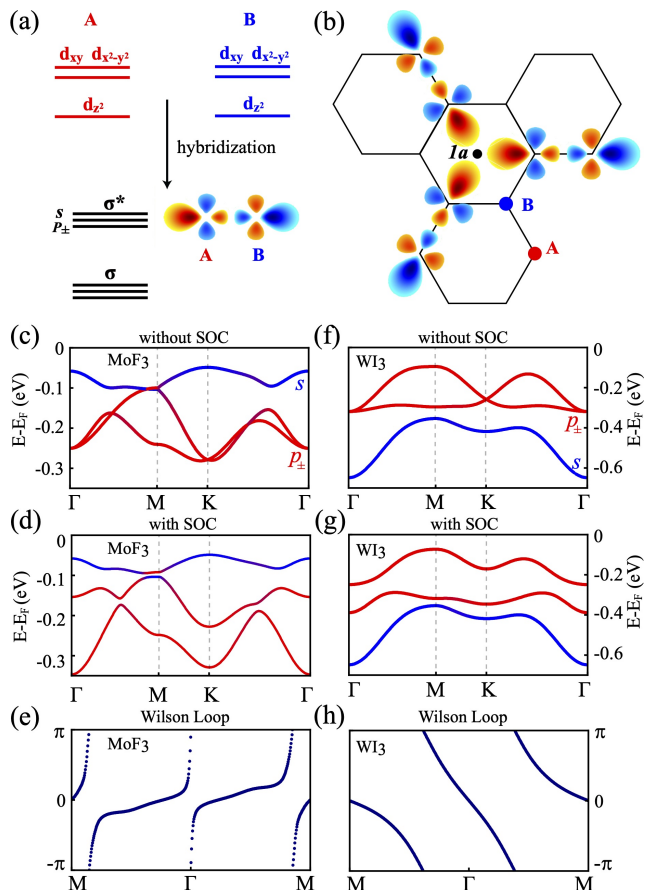


FIG. 3. (a) Schematics of sd^2 hybrid orbitals and antibonding σ^* state. (b) Triangular lattice formed by σ^* state at Wyckoff position $1a$ as basis in a hexagonal lattice. (c)-(e) MoF_3 , (f)-(h) WI_3 . The band structure of tight-binding model with and without SOC, and Wilson loop for the highest valence band. The irreducible representation at high-symmetry points of Brillouin zone boundary in (c) and (f) are consistent with that in Fig. 3(a) and 3(e), respectively. s and p type bands are labeled as blue and red, respectively.

The different topology of FCB in monolayer MoF_3 and WI_3 is rooted in SOC, which can be explicitly written as

$$\begin{aligned} \mathcal{H}_{\text{soc}} = & \lambda_1 \sum_i (b_i^\dagger b_i - c_i^\dagger c_i) + \lambda_2 \sum_{\langle ij \rangle} [(b_j^\dagger b_i - c_j^\dagger c_i) + \text{H.c.}] \\ & + \lambda_3 \sum_{\langle ij \rangle} [(e^{-i\theta_{ij}} b_j^\dagger a_i - e^{i\theta_{ij}} c_j^\dagger a_i) + \text{H.c.}], \end{aligned} \quad (1)$$

where (a_i, b_i, c_i) represent annihilation operators at site i for (s, p_+, p_-) orbitals, $\lambda_{1,2,3}$ are SOC parameters from atomic SOC term as $\lambda_{\text{so}} \boldsymbol{\ell} \cdot \boldsymbol{\sigma} = \lambda_{\text{so}} (\ell_+ \sigma_- + \ell_- \sigma_+) / 2 + \lambda_{\text{so}} \ell_z \sigma_z$. $\lambda_1 = \lambda_{\text{so}}$ is from the last term, and $\lambda_{2,3}$ are from the first term together with orbital hopping and hybridization. For spin polarized band inversion with same spin here, $\lambda_{2,3} \sim \lambda_{\text{so}}^2 / \Delta E$, namely, second order process, where ΔE is the energy difference between intermediate states and (s, p_{\pm}) orbitals, and is of the order of 1 eV.

$\langle ij \rangle$ denotes the nearest-neighbor sites, θ_{ij} is the angle between x axis and direction from site i to j . The topology of FCB in MoF_3 is the effective s - p band inversion around M points, where an SOC gap is opened by the λ_3 term in Eq. (1). The triple M points related by C_{3z} symmetry leads to higher Chern number $\mathcal{C} = +3$ of FCB, the sign of which is determined by $\text{sgn}(\lambda_3)$. The λ_{so} and λ_2 terms only affect the topology of the p_{\pm} bands. All of these are consistent with the Wilson loop calculations for the highest valence band shown in Fig. 3(d). While for p_{\pm} orbitals in WI_3 , the first and second terms in Eq. (1) lead to gap opening at quadratic band touching point Γ and Dirac point K , where $\Delta_{\Gamma} = 2\lambda_{\text{so}} + 12\lambda_2$ and $\Delta_K = 2\lambda_{\text{so}} - 4\lambda_2$. \mathcal{I} symmetry indicates that Chern number for the first valence band is $\mathcal{C} = -2$ or $\mathcal{C} = 0$ which depends on $\text{sgn}(\Delta_{\Gamma}\Delta_K) = -1$ or $\text{sgn}(\Delta_{\Gamma}\Delta_K) = +1$, respectively. To get the topological nontrivial band, $|\lambda_2| > |\lambda_{\text{so}}|/2$ (if $\text{sgn}[\lambda_{\text{so}}\lambda_2] = 1$) or $|\lambda_2| > |\lambda_{\text{so}}|/6$ (if $\text{sgn}[\lambda_{\text{so}}\lambda_2] = -1$) must be satisfied. Usually $|\lambda_2| \ll |\lambda_{\text{so}}|$, however the latter condition is fulfilled for WI_3 with strong SOC, which is consistent with the Wilson loop calculation in Fig. 3(h).

Hofstadter butterfly of FCB— Finally, we study the Hofstadter butterfly and Landau levels of FCB for MoF_3 and WI_3 in Fig. 4. Since FCB is not exactly flat and the valence band top at K in MoF_3 and at M in WI_3 have almost vanishing Berry curvature, the Landau levels at small Φ/Φ_0 around Fermi level are the same as that of trivial band structure. Moreover, the Hofstadter topology in Fig. 4 shows that at $\nu = -1$ filling, there must be an insulator-metal transition by adding magnetic field. This can be understood from Streda formula $\partial\rho/\partial B = \mathcal{C}/\Phi_0$, namely, the filling of a state with fixed a nonzero Chern number changes as the flux is increased. Thus at fixed filling, the Chern insulator gap must have discontinuity at $\Phi = 0$ and finite Φ [74, 75].

Discussions— The key ingredient for FCB with higher Chern number here is rooted in the sd^2 hybridization, which transform the atomic d orbitals on hexagonal lattice into (s, p_+, p_-) orbitals on triangular lattice. In fact, sd^2 hybridization on hexagonal lattice may also transform into s orbital on emergent kagome lattice [76, 77]. As two representative examples, MoF_3 and WI_3 have quite different origin of topology within (s, p_+, p_-) orbitals. MoF_3 is from band inversion, where the topological gap opening at a finite wave vector δk away from band inversion point is smaller compared to atomic SOC $E_g/E_{\text{inv}} \sim \delta ka$. WI_3 is from atomic SOC gap opening at Dirac point. Indeed the gap from FCB to nearby band in MoF_3 (~ 17 meV) is smaller than that in WI_3 (~ 50 meV). Interestingly, both the topology and magnetism in these materials are solely from d orbitals. We anticipate the physics in transition metal trihalide is general, which applies to a large class of materials with $P\text{-}31m$ symmetry.

The interaction energy scale is generated from the lattice constant as $U \sim e^2/\epsilon a$, where ϵ is the dielectric con-

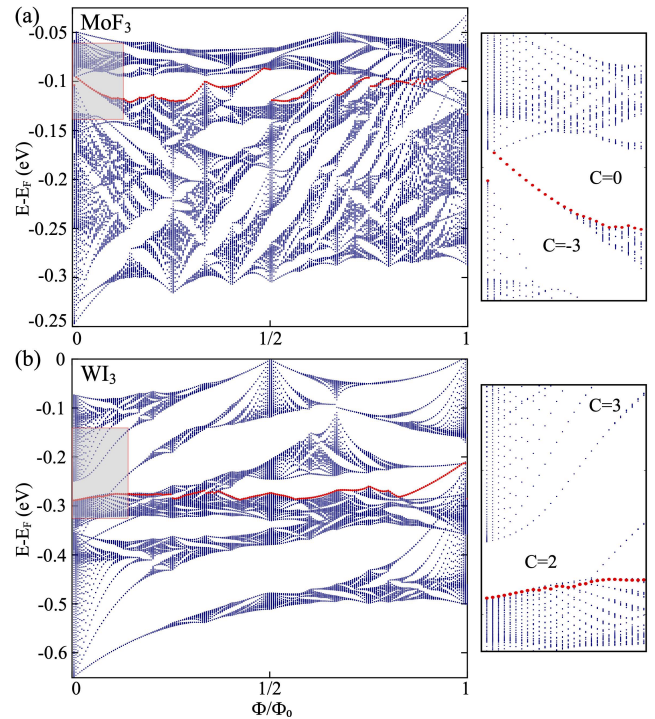


FIG. 4. Hofstadter butterfly of the three-band model for (a) MoF_3 and (b) WI_3 , where Φ/Φ_0 is the magnetic flux per unit cell. The $\nu = -1$ filling is labeled by red dots. The grey parts are enlarged on the right panel.

stant. We choose $\epsilon = 5$, then $U \sim 0.5$ eV. For isolated FCB in MoF_3 and WI_3 , the bandwidth is significantly smaller than the Coulomb repulsion energy $U/W \gtrsim 2$. Thus these 2D materials offer new promising platforms for exotic correlated states. Specifically, we consider the trace condition for FCB that have been proposed to probe the suitability of a band to realize fractionalized phases at partial filling. Two geometric indicators are defined as

$$(\delta\mathcal{B})^2 \equiv \frac{\Omega_{\text{BZ}}}{4\pi^2} \int_{\text{BZ}} d^2\mathbf{k} \left(\mathcal{B}(\mathbf{k}) - \frac{2\pi\mathcal{C}}{\Omega_{\text{BZ}}} \right)^2, \quad (2)$$

$$\text{T} \equiv \frac{1}{2\pi} \int_{\text{BZ}} d^2\mathbf{k} [\text{Tr}(g_{\mu\nu}(\mathbf{k})) - |\mathcal{B}(\mathbf{k})|], \quad (3)$$

where $\delta\mathcal{B}$ describes the fluctuations of Berry curvature and T (non-negative) is the average trace condition violation. $g_{\mu\nu}(\mathbf{k}) \equiv \text{Re}(\eta^{\mu\nu})$ is the Fubini-Study metric, $\mathcal{B}(\mathbf{k}) \equiv -2\text{Im}(\eta^{xy})$ is Berry curvature, $\eta^{\mu\nu}(\mathbf{k}) \equiv \langle \partial^\mu u_{\mathbf{k}} | (1 - |u_{\mathbf{k}}\rangle\langle u_{\mathbf{k}}|) | \partial^\nu u_{\mathbf{k}} \rangle$ is the quantum geometric tensor. $\mathcal{C} \equiv (1/2\pi) \int d^2\mathbf{k} \mathcal{B}(\mathbf{k})$, Ω_{BZ} is area of Brillouin zone. A Chern band with $\text{T} = 0$ may be exactly mapped to a Landau level, which is said to be “ideal” for the realization of fractional Chern insulators [12–17]. For MoF_3 , $\delta\mathcal{B} = 10.04$ and $\text{T} = 2.98$. For WI_3 , $\delta\mathcal{B} = 1.73$ and $\text{T} = 0.1$. It is noteworthy that T value is comparable with those identified in moiré materials [14, 78, 79]. Together with the higher Chern number, the systems may

lead to exotic topologically nontrivial many body states.

Furthermore, by constructing homobilayers or heterobilayers consisting of MoF_3/WI_3 or with other 2D semiconductors, one may further tune the bandwidth as well as Chern number of the minibands from isolated Chern band. Also, by stacking MoF_3 or WI_3 on superconducting 2D materials, such as NbSe_2 , the chiral topological superconducting phase may be achieved [80]. We leave all these for future studies.

In summary, our work uncover a class of natural materials of monolayer transition metal trihalides MoF_3 and WX_3 in the space group $P\text{-}31m$, which host isolated nearly flat higher Chern bands with $\mathcal{C} = +3$ and $\mathcal{C} = -2$, respectively. This offers new platforms to explore correlated phenomena driven by flat Chern bands with higher Chern number. We hope this theoretical work could aid the investigations of flat Chen bands in transition metal compounds.

Acknowledgment. This work is supported by the National Key Research Program of China under Grant No. 2019YFA0308404, the Natural Science Foundation of China through Grants No. 12350404 and No. 12174066, the Innovation Program for Quantum Science and Technology through Grant No. 2021ZD0302600, the Science and Technology Commission of Shanghai Municipality under Grant No. 23JC1400600, Shanghai Municipal Science and Technology Major Project under Grant No. 2019SHZDZX01. K.B. and H.W. contributed equally to this work.

* Corresponding author: wjingphys@fudan.edu.cn

- [1] Jiaqi Cai, Eric Anderson, Chong Wang, Xiaowei Zhang, Xiaoyu Liu, William Holtzmann, Yinong Zhang, Fengren Fan, Takashi Taniguchi, Kenji Watanabe, Ying Ran, Ting Cao, Liang Fu, Di Xiao, Wang Yao, and Xiaodong Xu, “Signatures of fractional quantum anomalous hall states in twisted mote₂,” *Nature* **622**, 63–68 (2023).
- [2] Yihang Zeng, Zhengchao Xia, Kaifei Kang, Jiacheng Zhu, Patrick Knüppel, Chirag Vaswani, Kenji Watanabe, Takashi Taniguchi, Kin Fai Mak, and Jie Shan, “Thermodynamic evidence of fractional chern insulator in moiré mote₂,” *Nature* **622**, 69–73 (2023).
- [3] Heonjoon Park, Jiaqi Cai, Eric Anderson, Yinong Zhang, Jiayi Zhu, Xiaoyu Liu, Chong Wang, William Holtzmann, Chaowei Hu, Zhaoyu Liu, Takashi Taniguchi, Kenji Watanabe, Jiun-Haw Chu, Ting Cao, Liang Fu, Wang Yao, Cui-Zu Chang, David Cobden, Di Xiao, and Xiaodong Xu, “Observation of fractionally quantized anomalous hall effect,” *Nature* **622**, 74–79 (2023).
- [4] Fan Xu, Zheng Sun, Tongtong Jia, Chang Liu, Cheng Xu, Chushan Li, Yu Gu, Kenji Watanabe, Takashi Taniguchi, Bingbing Tong, Jinfeng Jia, Zhiwen Shi, Shengwei Jiang, Yang Zhang, Xiaoxue Liu, and Tingxin Li, “Observation of integer and fractional quantum anomalous hall effects in twisted bilayer mote₂,” *Phys. Rev. X* **13**, 031037 (2023).
- [5] Zhengguang Lu, Tonghang Han, Yuxuan Yao, Aidan P. Reddy, Jixiang Yang, Junseok Seo, Kenji Watanabe, Takashi Taniguchi, Liang Fu, and Long Ju, “Fractional quantum anomalous hall effect in multilayer graphene,” *Nature* **626**, 759–764 (2024).
- [6] Evelyn Tang, Jia-Wei Mei, and Xiao-Gang Wen, “High-temperature fractional quantum hall states,” *Phys. Rev. Lett.* **106**, 236802 (2011).
- [7] Kai Sun, Zhengcheng Gu, Hosho Katsura, and S. Das Sarma, “Nearly flatbands with nontrivial topology,” *Phys. Rev. Lett.* **106**, 236803 (2011).
- [8] Titus Neupert, Luiz Santos, Claudio Chamon, and Christopher Mudry, “Fractional quantum hall states at zero magnetic field,” *Phys. Rev. Lett.* **106**, 236804 (2011).
- [9] N. Regnault and B. Andrei Bernevig, “Fractional chern insulator,” *Phys. Rev. X* **1**, 021014 (2011).
- [10] D. N. Sheng, Zheng-Cheng Gu, Kai Sun, and L. Sheng, “Fractional quantum hall effect in the absence of landau levels,” *Nature Commun.* **2**, 389 (2011).
- [11] S. A. Parameswaran, R. Roy, and S. L. Sondhi, “Fractional chern insulators and the W_∞ algebra,” *Phys. Rev. B* **85**, 241308 (2012).
- [12] Rahul Roy, “Band geometry of fractional topological insulators,” *Phys. Rev. B* **90**, 165139 (2014).
- [13] Martin Claassen, Ching Hua Lee, Ronny Thomale, Xiao-Liang Qi, and Thomas P. Devereaux, “Position-momentum duality and fractional quantum hall effect in chern insulators,” *Phys. Rev. Lett.* **114**, 236802 (2015).
- [14] Patrick J. Ledwith, Grigory Tarnopolsky, Eslam Khalaf, and Ashvin Vishwanath, “Fractional chern insulator states in twisted bilayer graphene: An analytical approach,” *Phys. Rev. Res.* **2**, 023237 (2020).
- [15] Jie Wang, Jennifer Cano, Andrew J. Millis, Zhao Liu, and Bo Yang, “Exact landau level description of geometry and interaction in a flatband,” *Phys. Rev. Lett.* **127**, 246403 (2021).
- [16] S. A. Parameswaran, R. Roy, and S. L. Sondhi, “Fractional quantum hall physics in topological flat bands,” *Comptes Rendus. Physique* **14**, 816–839 (2013).
- [17] Patrick J. Ledwith, Ashvin Vishwanath, and Daniel E. Parker, “Vortexability: A unifying criterion for ideal fractional chern insulators,” *Phys. Rev. B* **108**, 205144 (2023).
- [18] Zhao Liu and Emil J. Bergholtz, “Recent developments in fractional chern insulators,” in *Encyclopedia of Condensed Matter Physics (Second Edition)*, edited by Tapash Chakraborty (Academic Press, Oxford, 2024) 2nd ed., pp. 515–538.
- [19] Sebastiano Peotta and Päivi Törmä, “Superfluidity in topologically nontrivial flat bands,” *Nature Commun.* **6**, 1–9 (2015).
- [20] Y. Cao, V. Fatemi, S. Fang, K. Watanabe, T. Taniguchi, E. Kaxiras, and P. Jarillo-Herrero, “Unconventional superconductivity in magic-angle graphene superlattices,” *Nature* **556**, 43 (2018).
- [21] Xiang Hu, Timo Hyart, Dmitry I. Pikulin, and Enrico Rossi, “Geometric and conventional contribution to the superfluid weight in twisted bilayer graphene,” *Phys. Rev. Lett.* **123**, 237002 (2019).
- [22] A. Julku, T. J. Peltonen, L. Liang, T. T. Heikkilä, and P. Törmä, “Superfluid weight and berezinskii-kosterlitz-thouless transition temperature of twisted bilayer graphene,” *Phys. Rev. B* **101**, 060505 (2020).

- [23] Fang Xie, Zhida Song, Biao Lian, and B. Andrei Bernevig, “Topology-bounded superfluid weight in twisted bilayer graphene,” *Phys. Rev. Lett.* **124**, 167002 (2020).
- [24] A Mielke, “Ferromagnetic ground states for the hubbard model on line graphs,” *J. Phys. A* **24**, L73–L77 (1991).
- [25] A Mielke, “Ferromagnetism in the hubbard model on line graphs and further considerations,” *J. Phys. A* **24**, 3311–3321 (1991).
- [26] Hal Tasaki, “From Nagaoka’s Ferromagnetism to Flat-Band Ferromagnetism and Beyond: An Introduction to Ferromagnetism in the Hubbard Model,” *Prog. Theor. Phys.* **99**, 489–548 (1998).
- [27] Congjun Wu, Doron Bergman, Leon Balents, and S. Das Sarma, “Flat bands and wigner crystallization in the honeycomb optical lattice,” *Phys. Rev. Lett.* **99**, 070401 (2007).
- [28] Doron L. Bergman, Congjun Wu, and Leon Balents, “Band touching from real-space topology in frustrated hopping models,” *Phys. Rev. B* **78**, 125104 (2008).
- [29] Zheng Liu, Feng Liu, and Yong-Shi Wu, “Exotic electronic states in the world of flat bands: From theory to material,” *Chin. Phys. B* **23**, 077308 (2014).
- [30] Jun-Won Rhim and Bohm-Jung Yang, “Classification of flat bands according to the band-crossing singularity of bloch wave functions,” *Phys. Rev. B* **99**, 045107 (2019).
- [31] Da-Shuai Ma, Yuanfeng Xu, Christie S. Chiu, Nicolas Regnault, Andrew A. Houck, Zhida Song, and B. Andrei Bernevig, “Spin-orbit-induced topological flat bands in line and split graphs of bipartite lattices,” *Phys. Rev. Lett.* **125**, 266403 (2020).
- [32] Dumitru Călugăru, Aaron Chew, Luis Elcoro, Yuanfeng Xu, Nicolas Regnault, Zhi-Da Song, and B. Andrei Bernevig, “General construction and topological classification of crystalline flat bands,” *Nature Phys.* **18**, 185–189 (2022).
- [33] Hang Liu, Sheng Meng, and Feng Liu, “Screening two-dimensional materials with topological flat bands,” *Phys. Rev. Mater.* **5**, 084203 (2021).
- [34] Nicolas Regnault, Yuanfeng Xu, Ming-Rui Li, Da-Shuai Ma, Milena Jovanovic, Ali Yazdani, Stuart SP Parkin, Claudia Felser, Leslie M Schoop, N Phuan Ong, Robert J. Cava, Luis Elcoro, Zhi-Da Song, and B. Andrei Bernevig, “Catalogue of flat-band stoichiometric materials,” *Nature* **603**, 824–828 (2022).
- [35] Zheng Liu, Zheng-Fei Wang, Jia-Wei Mei, Yong-Shi Wu, and Feng Liu, “Flat chern band in a two-dimensional organometallic framework,” *Phys. Rev. Lett.* **110**, 106804 (2013).
- [36] Masahiko G. Yamada, Tomohiro Soejima, Naoto Tsuji, Daisuke Hirai, Mircea Dincă, and Hideo Aoki, “First-principles design of a half-filled flat band of the kagome lattice in two-dimensional metal-organic frameworks,” *Phys. Rev. B* **94**, 081102 (2016).
- [37] Zhenyu Sun, Hui Zhou, Cuixiang Wang, Shiv Kumar, Daiyu Geng, Shaosheng Yue, Xin Han, Yuya Haraguchi, Kenya Shimada, Peng Cheng, Lan Chen, Youguo Shi, Kehui Wu, Sheng Meng, and Baojie Feng, “Observation of topological flat bands in the kagome semiconductor nb3cl8,” *Nano Lett.* **22**, 4596–4602 (2022).
- [38] Shunye Gao, Shuai Zhang, Cuixiang Wang, Shaohua Yan, Xin Han, Xuecong Ji, Wei Tao, Jingtong Liu, Tiantian Wang, Shuaikang Yuan, Gexing Qu, Ziyuan Chen, Yongzhao Zhang, Jierui Huang, Mojun Pan, Shiyu Peng, Yong Hu, Hang Li, Yaobo Huang, Hui Zhou, Sheng Meng, Liu Yang, Zhiwei Wang, Yugui Yao, Zhiguo Chen, Ming Shi, Hong Ding, Huaixin Yang, Kun Jiang, Yunliang Li, Hechang Lei, Youguo Shi, Hongming Weng, and Tian Qian, “Discovery of a single-band mott insulator in a van der waals flat-band compound,” *Phys. Rev. X* **13**, 041049 (2023).
- [39] Minghu Pan, Xin Zhang, Yinong Zhou, Pengdong Wang, Qi Bian, Hang Liu, Xingyue Wang, Xiaoyin Li, Aixi Chen, Xiaoxu Lei, Shaojian Li, Zhengwang Cheng, Zhibin Shao, Haoxuan Ding, Jianzhi Gao, Fangsen Li, and Feng Liu, “Growth of mesoscale ordered two-dimensional hydrogen-bond organic framework with the observation of flat band,” *Phys. Rev. Lett.* **130**, 036203 (2023).
- [40] Anupam Bhattacharya, Ivan Timokhin, Ruchira Chatterjee, Qian Yang, and Artem Mishchenko, “Deep learning approach to genome of two-dimensional materials with flat electronic bands,” *npj Comput. Mater.* **9**, 101 (2023).
- [41] Paul M. Neves, Joshua P. Wakefield, Shiang Fang, Haimi Nguyen, Linda Ye, and Joseph G. Checkelsky, “Crystal net catalog of model flat band materials,” *npj Comput. Mater.* **10**, 39 (2024).
- [42] Hongrun Zhang, Zhijian Shi, Zhicheng Jiang, Ming Yang, Jingwei Zhang, Ziyuan Meng, Tonghua Hu, Fucai Liu, Long Cheng, Yong Xie, , Jincheng Zhuang, Haifeng Feng, Weichang Hao, Dawei Shen, and Yi Du, “Topological flat bands in 2d breathing-kagome lattice nb3tecl7,” *Adv. Mater.* **35**, 2301790 (2023).
- [43] Jingyi Duan, Da-Shuai Ma, Run-Wu Zhang, Wei Jiang, Zeyang Zhang, Chaoxi Cui, Zhi-Ming Yu, and Yugui Yao, “Cataloging high-quality two-dimensional van der waals materials with flat bands,” *Adv. Funct. Mater.* , 2313067 (2024).
- [44] Linda Ye, Shiang Fang, Mingu Kang, Josef Kaufmann, Yonghun Lee, Caolan John, Paul M. Neves, S. Y. Frank Zhao, Jonathan Denlinger, Chris Jozwiak, Aaron Bostwick, Eli Rotenberg, Efthimios Kaxiras, David C. Bell, Oleg Janson, Riccardo Comin, and Joseph G. Checkelsky, “Hopping frustration-induced flat band and strange metallicity in a kagome metal,” *Nature Phys.* (2024), 10.1038/s41567-023-02360-5.
- [45] Jia-Xin Yin, Biao Lian, and M Zahid Hasan, “Topological kagome magnets and superconductors,” *Nature* **612**, 647–657 (2022).
- [46] Maissam Barkeshli and Xiao-Liang Qi, “Topological nematic states and non-abelian lattice dislocations,” *Phys. Rev. X* **2**, 031013 (2012).
- [47] Zhao Liu, Emil J. Bergholtz, Heng Fan, and Andreas M. Läuchli, “Fractional chern insulators in topological flat bands with higher chern number,” *Phys. Rev. Lett.* **109**, 186805 (2012).
- [48] Yi-Fei Wang, Hong Yao, Chang-De Gong, and D. N. Sheng, “Fractional quantum hall effect in topological flat bands with chern number two,” *Phys. Rev. B* **86**, 201101 (2012).
- [49] Gunnar Möller and Nigel R. Cooper, “Fractional chern insulators in harper-hofstadter bands with higher chern number,” *Phys. Rev. Lett.* **115**, 126401 (2015).
- [50] Jie Wang and Zhao Liu, “Hierarchy of ideal flatbands in chiral twisted multilayer graphene models,” *Phys. Rev. Lett.* **128**, 176403 (2022).
- [51] Patrick J. Ledwith, Ashvin Vishwanath, and Eslam Kha-

- laf, “Family of ideal chern flatbands with arbitrary chern number in chiral twisted graphene multilayers,” *Phys. Rev. Lett.* **128**, 176404 (2022).
- [52] Fa Wang and Ying Ran, “Nearly flat band with chern number $c = 2$ on the dice lattice,” *Phys. Rev. B* **84**, 241103 (2011).
- [53] Shuo Yang, Zheng-Cheng Gu, Kai Sun, and S. Das Sarma, “Topological flat band models with arbitrary chern numbers,” *Phys. Rev. B* **86**, 241112 (2012).
- [54] Bartholomew Andrews and Gunnar Möller, “Stability of fractional chern insulators in the effective continuum limit of harper-hofstadter bands with chern number $|c| > 1$,” *Phys. Rev. B* **97**, 035159 (2018).
- [55] Bartholomew Andrews, Titus Neupert, and Gunnar Möller, “Stability, phase transitions, and numerical breakdown of fractional chern insulators in higher chern bands of the hofstadter model,” *Phys. Rev. B* **104**, 125107 (2021).
- [56] Bartholomew Andrews, Mathi Raja, Nimit Mishra, Michael P. Zaletel, and Rahul Roy, “Stability of fractional chern insulators with a non-landau level continuum limit,” (2024), [arXiv:2310.05758 \[cond-mat.str-el\]](https://arxiv.org/abs/2310.05758).
- [57] M. I. Aroyo, J. M. Perez-mato, C. Capillas, E. Kroumova, S. Ivantchev, G. Madariaga, A. Kirov, and H. Wondratschek, “Bilbao crystallographic server: I. databases and crystallographic computing programs,” *Z. Kristallogr.* **221**, 15–27 (2006).
- [58] Asen Kirov, Cesar Capillas, J Perez-Mato, and Hans Wondratschek, “Bilbao crystallographic server. ii. representations of crystallographic point groups and space groups,” *Acta Crystallogr. Sect. B* **62**, 115–28 (2006).
- [59] Jorrit Kruthoff, Jan de Boer, Jasper van Wezel, Charles L. Kane, and Robert-Jan Slager, “Topological classification of crystalline insulators through band structure combinatorics,” *Phys. Rev. X* **7**, 041069 (2017).
- [60] M. G. Vergniory, L. Elcoro, Zhijun Wang, Jennifer Cano, C. Felser, M. I. Aroyo, B. Andrei Bernevig, and Barry Bradlyn, “Graph theory data for topological quantum chemistry,” *Phys. Rev. E* **96**, 023310 (2017).
- [61] L. Elcoro, Barry Bradlyn, Z. Wang, M. G. Vergniory, Jennifer Cano, C. Felser, B. Bernevig, D. Orobengoa, G. D. L. Flor, and M. Aroyo, “Double crystallographic groups and their representations on the bilbao crystallographic server,” *J. Appl. Crystallogr.* **50**, 1457 (2017).
- [62] Barry Bradlyn, L Elcoro, Jennifer Cano, MG Vergniory, Zhijun Wang, C Felser, MI Aroyo, and B Andrei Bernevig, “Topological quantum chemistry,” *Nature* **547**, 298 (2017).
- [63] G. Kresse and J. Furthmüller, “Efficient iterative schemes for ab initio total-energy calculations using a plane-wave basis set,” *Phys. Rev. B* **54**, 11169–11186 (1996).
- [64] Jianwei Sun, Adrienn Ruzsinszky, and John P. Perdew, “Strongly constrained and appropriately normed semilocal density functional,” *Phys. Rev. Lett.* **115**, 036402 (2015).
- [65] Aliaksandr V. Krukau, Oleg A. Vydrov, Artur F. Izmaylov, and Gustavo E. Scuseria, “Influence of the exchange screening parameter on the performance of screened hybrid functionals,” *J. Chem. Phys.* **125**, 224106 (2006).
- [66] See Supplemental Material for methods and technical details.
- [67] D. E. LaValle, R. M. Steele, M. K. Wilkinson, and H. L. Yakel Jr., “The preparation and crystal structure of molybdenum (iii) fluoride,” *J. Am. Chem. Soc.* **82**, 2433–2434 (1960).
- [68] F Averdunk and R Hoppe, “Zur kristallstruktur von mof3 [1],” *J. Less Common Met.* **161**, 135–140 (1990).
- [69] Tian Liu, Na Zhou, Xu Li, Guojun Zhu, Xiaolin Wei, and Juexian Cao, “Prediction of colossal magnetocrystalline anisotropy for transition metal triiodides,” *J. Phys.: Condens. Matter* **31**, 295801 (2019).
- [70] Renhao Deng, Hong Cui, Baogui Li, Huan Tang, Ying Chen, Hong Chen, and Hongkuan Yuan, “Exploring the heavy transition metal trihalide family: Two-dimensional magnetic materials with tunable band gap, huge magnetic anisotropy, and high-temperature magnetic ordering,” *Phys. Rev. Mater.* **6**, 024001 (2022).
- [71] Masood Ashraf Ali and Md Azaharuddin Ahmed, “W_i3 monolayer: Electronic band structure and magnetic anisotropy under an external electric field,” *J. Electron. Mater.* **52**, 1002–1012 (2023).
- [72] Daniel I. Khomskii, *Transition Metal Compounds* (Cambridge University Press, 2004).
- [73] Bevin Huang, Genevieve Clark, Efrén Navarro-Moratalla, Dahlia R. Klein, Ran Cheng, Kyle L. Seyler, Ding Zhong, Emma Schmidgall, Michael A. McGuire, David H. Cobden, Wang Yao, Di Xiao, Pablo Jarillo-Herrero, and Xiaodong Xu, “Layer-dependent ferromagnetism in a van der waals crystal down to the monolayer limit,” *Nature* **546**, 270–273 (2017).
- [74] Biao Lian, Fang Xie, and B. Andrei Bernevig, “Landau level of fragile topology,” *Phys. Rev. B* **102**, 041402 (2020).
- [75] Jonah Herzog-Arbeitman, Zhi-Da Song, Nicolas Regnault, and B. Andrei Bernevig, “Hofstadter topology: Noncrystalline topological materials at high flux,” *Phys. Rev. Lett.* **125**, 236804 (2020).
- [76] Miao Zhou, Zheng Liu, Wenmei Ming, Zhengfei Wang, and Feng Liu, “ sd^2 graphene: Kagome band in a hexagonal lattice,” *Phys. Rev. Lett.* **113**, 236802 (2014).
- [77] Zhaochen Liu, Huan Wang, and Jing Wang, “Magnetic moiré surface states and flat chern bands in topological insulators,” *Phys. Rev. B* **106**, 035114 (2022).
- [78] Chong Wang, Xiao-Wei Zhang, Xiaoyu Liu, Yuchi He, Xiaodong Xu, Ying Ran, Ting Cao, and Di Xiao, “Fractional chern insulator in twisted bilayer mote₂,” *Phys. Rev. Lett.* **132**, 036501 (2024).
- [79] Cheng Xu, Jiangxu Li, Yong Xu, Zhen Bi, and Yang Zhang, “Maximally localized wannier functions, interaction models, and fractional quantum anomalous hall effect in twisted bilayer mote₂,” *Proc. Natl. Acad. Sci. U.S.A.* **121**, e2316749121 (2024).
- [80] Jing Wang, Quan Zhou, Biao Lian, and Shou-Cheng Zhang, “Chiral topological superconductor and half-integer conductance plateau from quantum anomalous hall plateau transition,” *Phys. Rev. B* **92**, 064520 (2015).